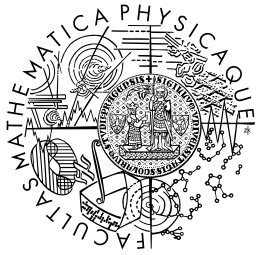

FACULTY
OF MATHEMATICS
AND PHYSICS
Charles University

BACHELOR THESIS

Sebastian Jakš

The Young Star Clusters in the Galactic Centre

Astronomical Institute of Charles University

Supervisor of the bachelor thesis:	RNDr. Jaroslav Haas, Ph.D.
Study programme:	Physics
Study branch:	General Physics

Prague 2017

I declare that I carried out this bachelor thesis independently, and only with the cited sources, literature and other professional sources.

I understand that my work relates to the rights and obligations under the Act No. 121/2000 Sb., the Copyright Act, as amended, in particular the fact that the Charles University in Prague has the right to conclude a license agreement on the use of this work as a school work pursuant to Section 60 subsection 1 of the Copyright Act.

In Prague date 19.7.2017 Sebastian Jakš

Title: The Young Star Clusters in the Galactic Centre

Author: Sebastian Jakš

Department: Astronomical Institute of Charles University

Supervisor: RNDr. Jaroslav Haas, Ph.D., Astronomical Institute of Charles University

Abstract: In addition to three massive star clusters – Arches, Quintuplet, Nuclear Star Cluster – the Galactic Centre hosts a significant number of isolated stars. It has been proposed that at least some of these stars were formed inside one of the three clusters and, subsequently, ejected out of them during their dynamical evolution. In this work, I investigate the dependence of this complex dynamical process for the Arches cluster upon its unknown line-of-sight distance by means of numerical N-body modelling. It turns out that both the dissipation rate of the Arches and spatial distribution of the ejected stars differs significantly if various values of the line-of-sight distance are considered. In the context of this finding, I critically evaluate the approach of Habibi et al. (2014) who assumed the Arches cluster to be 100 pc in front of the Galactic Centre when modelling its contribution to the observed isolated stars.

Keywords: Arches, galactic centre, star clusters, isolated stars

I would like to thank my thesis advisor RNDr. Jaroslav Haas, Ph.D. for his patience and invaluable advice during my work on this thesis. I would also like to thank Kathleen Winslow for helping me resolve language issues. Finally, I must express my gratitude to my family and to my girlfriend for providing me with support and encouragement. This accomplishment would not have been possible without them. Thank you.

Contents

Introduction

The Galactic Centre region (GC region) hosts three star clusters – Arches, Quintuplet and Nuclear Star Cluster. Besides them, several isolated massive stars have been observed in that region (Wang et al., 2010; Dong et al., 2011; Mauerhan et al., 2010a; Mauerhan et al., 2010b). The origin of those stars is not yet conclusively explained. One possibility is that they formed inside one of the three observed clusters and were ejected during the clusters' evolution.

Habibi et al. (2014) performed a set of simulations of Arches and Quintuplet clusters in a simplyfied GC potential in order to see if those clusters could produce enough free stars to explain the observed ones and if their distribution would be similar to the one seen on the sky. Their best model produced a similar distribution of free stars as is actually observed – it reproduced the two strips of stars (tidal arms) parallel to the galactic plane. They report that their models reproduce up to 80 % of observed heavy stars in the 20 pc neighbourhood of the Arches cluster and 60 % of stars in the 80 pc radius. Both Arches' tidal arms stretched out to 20 pc from the cluster's centre.

The positions of the Arches and Quintuplet clusters on the plane of the sky are very well known; however their position along the line of sight from the Galactic Centre (GC) cannot be determined with enough precision in order to reconstruct the clusters' orbit, since the uncertainities in determining distances at the GC distance of 8 kpc are of the order of 10^2-10^3 pc. Nevertheless, some constraints on their current position can be put in place. The Arches cluster seems to have smaller extinction than the mean extinction of the GC, suggesting that the Arches cluster is currently in front of the GC, which places it on the more probable prograde orbit (see Stolte et al., 2008). Also the cluster's interaction with the dense parts of the central molecular cloud (Wang et al., 2006, Lang et al., 2003, Stolte et al., 2008) suggests that the cluster is relatively close to the GC, probably not more than 200 pc. Habibi et al. (2014) assumed the line-of-sight distance to be -100 pc (100 pc in front of the GC) for their simulations. The question is, how would the expected contribution of the clusters to the free star population change between different trajectories corresponding to different line-of-sight distances.

In this thesis I perform several simulations of the Arches cluster with similar initial conditions as the model of Habibi et al. (2014) on different trajectories corresponding to line-of-sight distances between 0 and -200 pc and look at what portion of the cluster's mass is being ejected on different trajectories. I also study and comare the length and width of the cluster's tidal arms.

The simulations performed within this thesis will show whether and how much it is crucial to know the present-day line-of-sight distance of the clusters in order to explain the origin of the free stars in the galactic centre.

1. Star clusters

Star clusters are aggregations of stars of various size, shape, age, composition and origin. They are being observed not only inside our own galaxy, but also in its close surroundings and even in some neighbouring galaxies.

1.1 Types of star clusters

We distinguish three main types of stellar clusters:

Open clusters are young clusters that can be found in star-forming regions of our galaxy (mainly in spiral arms). They tipically consist of no more than a few thousand stars. Their mass ranges between 10 to $10^4\,M_\odot$ with a mean value of $300\,M_\odot$ (Binney and Tremaine, 2008). There are approximately 1000 open clusters being observed in our galaxy (out of the expected total number of $10^5\,M_\odot$). The mean core radius of those clusters is 1.3 pc (Nilakshi et al., 2002). Their central density is relatively low ($10\,M_\odot/pc^3$ on average – Binney and Tremaine, 2008)), so they are weakly gravitationally bound and therefore unstable. The typical lifetime of an open cluster does not exceed a few hundred million years. They consist of young stars that formed simultaneously by the collapse of a primordial dust cloud.

Globular clusters are larger and older than open clusters. They contain up to several million stars that are strongly gravitationally bound, which makes this type of cluster more stable. The average core density of globular clusters is $10^4\,M_\odot/pc^3$ (Binney and Tremaine, 2008), significantly higher than in the case of open clusters. Their average mass is $2 \cdot 10^5\,\mathrm{M}_\odot$ (Binney and Tremaine, 2008). They can be found at the peripheries of our galaxy (and other galaxies as well). Our galaxy hosts aproximately 150 globular clusters. Their origin dates back to the time of the formation of our galaxy (more than ten billion years) so they consist mostly of old stars.

Nuclear star clusters are located at the centres of galaxies. Their masses are typically between 10^6 and $10^7\,\mathrm{M}_\odot$ and their sizes between 2 and 5 pc (Böker, 2010). In some cases they surround a supermassive black hole (SMBH), which then influences their dynamics. Our galaxy also hosts this type of cluster - Nuclear Star Cluster (NSC).

Arches and Quintuplet are star clusters orbiting the centre of our galaxy. They do not belong to either of the three categories mentioned above. They have masses of 10^3 - $10^4\,\mathrm{M}_\odot$, so they fall into the open cluster category, but they are much more dense and more strongly gravitationally bound. Their dynamics are probably strongly influenced by extreme conditions in the galactic centre, especially by the strong external potential. They are very young (only several Myrs) and contain a significant portion of heavy stars. More information about those clusters along with the NSC will be provided in the second chapter.

1.2 Properties of star clusters

Star clusters can be described by several basic quantities:

The first and most obvious quantity is the number of stars in the cluster N. As mentioned above, this number can vary between several orders of magnitude, from 10^1 up to 10^6.

Another property is the total mass of the cluster M and the distribution of masses of individual stars. This can be described by a so-called initial or present-day mass function (IMF/PDMF):

$$dN = N\xi(m)\mathrm{d}m \tag{1.1}$$

where m is the mass of a star and $\xi(m)$ is a probability density function describing the distribution of stellar masses within the cluster population. The IMF describes the cluster at the time of its formation. The PDMF can differ from the IMF because of stellar evolution and dynamical evolution of the cluster, which will be described below. The equation (1.1) often takes a power-law form:

$$dN = Am^{\alpha}\mathrm{d}m \tag{1.2}$$

where A is a scaling parameter. One of the often adopted forms of the IMF comes from Salpeter (1955) with the exponent:

$$\alpha = -2.35 \tag{1.3}$$

The negative exponent means that lighter stars predominate over heavy ones. This form of the IMF is a good approximation for stars with masses greater than approximately $0.5\,M_{\odot}$. Observational data is mainly consistent with the hypothesis that the IMF is invariant among different populations of stars formed in different environments (Binney and Tremaine, 2008; Bastian et al., 2010). It is however unclear whether this IMF holds in the case of GC environment. Some studies suggest a flatter MF for the clusters at the GC region (see for example Figer et al., 1999a; Stolte et al., 2002), while others give results compatible with the Salpeter MF (Hußmann et al., 2012; Hußmann, 2014; Habibi et al., 2013).

Another important property of a star cluster is its spacial disribution of mass. This distribution generates the potential in which the stars are moving in (neglecting the external potential). In the first approximation, where the cluster is spherical and symmetric in respect to its centre, the potential depends only on the distance from the centre of the cluster r.

Probably the simpliest potential is the point mass potential:

$$\Phi(r) = -\frac{\mathrm{G}M}{r} \tag{1.4}$$

Stars in that potential move on Keplerian orbits. This potential can be used for example as a first approximation for star clusters around supermassive black holes (SMBH) at the centres of a galaxies.

Another simple potential is generated by a homogeneous sphere of radius R and spacial mass density ρ:

$$\Phi(r) = \begin{cases} -\frac{2}{3}\pi\mathrm{G}\rho r^2, & r < R \\ (\frac{2R^2}{3} - \frac{4R^3}{3r})\pi\mathrm{G}\rho, & r \geq R. \end{cases} \tag{1.5}$$

A more realistic potential is given by the following two requirements: a) constant mass density near the centre of the cluster and b) rapidly decreasing density beyond a certain radius b. Those two characteristics are being observed for example in globular clusters (Plummer, 1911). A potential fulfilling those two requirements can take the following form:

$$\Phi(r) = -\frac{\mathrm{G}M}{\sqrt{r^2 + b^2}} \tag{1.6}$$

This is called the Plummer Model. b is called Plummer scale length and M is the total mass of the cluster. The corresponding mass distribution is:

$$\rho(r) = \frac{3M}{4\pi b^3}(1 + \frac{r^2}{b^2})^{\frac{5}{2}} \tag{1.7}$$

There are many more sophisticated density profiles. But for simplicity I have chosen the Plummer model for the following simulations.

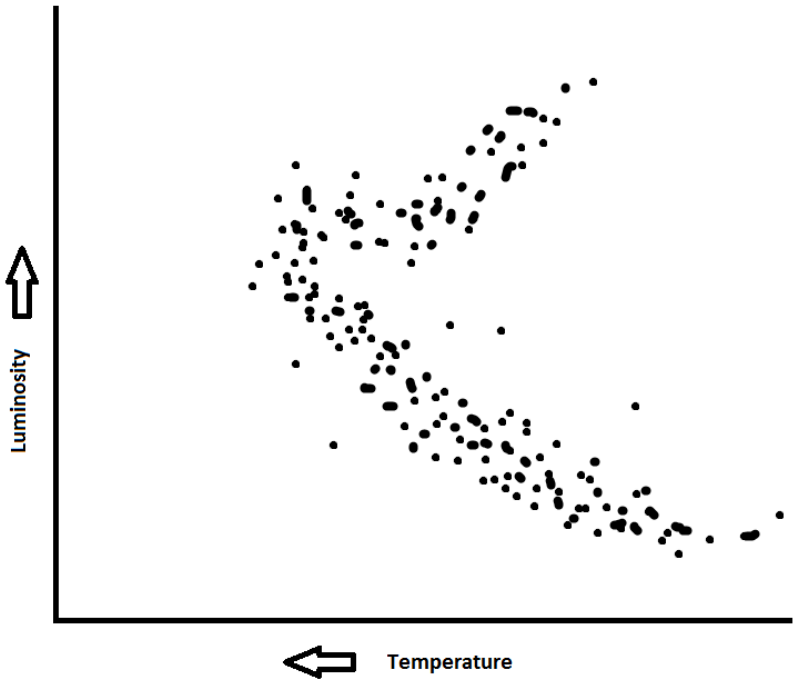

Figure 1.1: Example of an H-R diagram. The main sequence is interrupted at the turn-off point at the top-left part of the image.

Another important property is a cluster's current age. Assuming that all stars of the cluster formed simultaneously during one relatively short event, the cluster's age can be determined by examining and identifying different types of stars in the cluster and applying their theoretical evolutionary models. The simplest method consists in identifying the so-called turn-off point in the main sequence. Heavier stars burn hydrogen in their core faster than lighter ones and therefore leave the main sequence in a shorter time. The turn-off point is the point on the main sequence, where the stars are currently running out of

hydrogen and are leaving the main sequence. Their age can then be determined from their theoretical evolutionary models (and therefore the age of the entire cluster). The turn-off points can be well observed in so-called H-R diagrams. In these diagrams, one axis describes the star's luminosity and the second one its color or temperature. The main sequence then forms a line going from areas of high temperatures and luminosities towards the area of cooler and dimmer stars. If a turn-off point is present, then the area above a certain temperature limit is empty, and the stars of corresponding luminosities are moved towards the area of lower temperatures. Moreover, the whole main sequence line is moving in the H-R diagram while the cluster ages. Main sequence stars of the cluster then follow isochrones in the H-R diagram corresponding to different cluster ages. An example of an H-R diagram is in figure 1.1.

1.3 Dynamical evolution of star clusters

Stars moving in a potential generated by other stars belonging to the cluster do not maintain their original orbits for infinity. In a real cluster they encounter one another and exchange their energy and angular momentum, causing their orbits to change. This process, during which the cluster tends to reach a more stable form, is called relaxation. There are several processes that take place during the cluster's evolution. They are going to be described in this section.

1.3.1 Equipartition and mass segregation

During elastic encounters, the stars with higher kinetic energy tend to loose their energy in favour of less energetic stars and hence produce the equipartition of energy. Assuming we have a cluster with stars of various masses with comparable initial velocities, then this process will drain energy from the more massive stars and will transfer it to the lighter ones. Heavy stars will be loosing velocity and will be falling deeper to the cluster's centre, while lighter stars will be ejected to the outer parts of the cluster. Old evolved clusters will have dense cores composed of heavy stars and an outer shell made of light stars. If no other effects are taken into account, the core would continue to shrink down to the zero radius and infinite core density. This process is called core collapse. But in reality, the core will not collapse into a singularity. In a dense core, binary stars are going to be created by three-body encounters. After such an event, the resulting kinetic energy of the newly formed binary star (its centre of mass) plus the kinetic energy of the third star will be bigger than the sum of kinetic energies of the three input stars. This process adds energy to the collapsing core and eventually halts it's collapse.. Another process that adds energy to the core is the interactions of stars with hard binaries (see section *1.3.3*).

1.3.2 Star ejection and evaporation

If a star gains enough energy during an encounter, it can superate the escape velocity and leave the cluster. This event is called ejection. If a star gradually gains energy from several encounters, it can also finally gain enough speed to

escape the potential well of the cluster. This process by which the cluster spontaneously loses its mass is called evaporation. The cluster will naturally evaporate until there are only two stars left on a Keplerian orbit.

A rough estimate of the evaporation time (the time in which the cluster disintegrates due to evaporation) is given in Binney and Tremaine (2008):

$$t_{\mathrm{ev}} \approx 140\, t_{\mathrm{relax}} \tag{1.8}$$

where t_{relax} is the relaxation time (a characteristic of the system):

$$t_{\mathrm{relax}} \approx \frac{0.1N}{ln(N)}\, t_{\mathrm{cross}} \tag{1.9}$$

where t_{cross} is the crossing time – the time it takes a star with an average velocity to cross the cluster.

1.3.3 Effect of binaries

Binaries in the cluster can be divided into two groups by the mechanism of their birth:

1. Primordial binaries, which have been formed during the formation of the cluster directly from the pre-existing dust cloud.

2. Binaries formed later due to three-body encounters.

The mean time in which a binary star is formed by triple encounters is roughly (Binney and Tremaine, 2008):

$$t_{\mathrm{bin}} \approx 10 t_{\mathrm{relax}} N^2 ln(N) \tag{1.10}$$

This time exceeds significantly the evaporation time if $N>10$; therefore the count of those binaries is negligible in larger clusters. However, primordial binaries can influence the cluster's development significantly.

Binaries interact with other cluster members and exchange energy with them. We distinguish two kinds of binaries based on their internal energy E:

1. **Soft binaries** - if the absolute value of their internal energy is lower than the typical kinetic energy within the cluster. If the binary is very soft, its internal kinetic energy is smaller than the average kinetic energy of surrounding cluster stars, and due to equipartition, the binary star drains energy from the cluster by encounters with other star members, becomes even softer and finally it desintegrates (see Binney and Tremaine, 2008). However, the total energy exchanged between a soft binary and other stars does not exceed the average kinetic energy of a cluster member, so the soft binaries do not affect the cluster's development significantly.

2. **Hard binaries** - if the absolute value of their internal energy is higher than the typical kinetic energy within the cluster. Those binaries generally lose their internal energy to the cluster and become even harder, until they are ejected from the system (Binney and Tremaine, 2008). This energy exchange can significantly slow down the so-called core collapse (see section *1.3.1*) since it continues to supply the energy to the degenerated core. When all hard binaries are ejected, the core collapse continues.

1.3.4 Tidal stripping

When an object of non-zero size is placed in a central potential, it experiences tidal forces. This is because the gradient vector of that potential at distinct parts of the object have different magnitude and direction. The object is then being squeezed or stretched. This effect can be observed, for example, in moons orbiting their mother planets. Io, one of Jupiter's moons, is so deformed by tidal forces as it travels along its elliptical orbit, that it causes volcanic activity. The tidal forces can be strong enough to destroy the moon entirely. When a cluster moves through an external central potential it undergoes similar disrupting effects. The forces acting on individual stars differ, causing some of them to leave the cluster – especially the ones near the outer and inner edge of the cluster (the nearest and furthermost points from the centre of the potential). Those stars then continue to move on a separate orbit in the potential. Some of them move on higher orbits corresponding to lower orbital periods; those stars will form a trail behind the original cluster. Other stars will go to lower orbits, forming a trail forward to the cluster (see figure 3.3). Those trails are called tidal streams or tidal arms. The disruption effects that the GC potential has on the clusters orbiting in it is not easy to predict, and hence they are being simulated in this thesis.

2. Galactic Centre

2.1 Our galaxy

Our galaxy is a spiral galaxy with the majority of stars concentrated in a relatively thin disc with a diameter of aproximately 10^5 ly ($1\,\mathrm{ly} \doteq 0.307\,\mathrm{pc}$) and total mass $M_{\mathrm{disc}} = (4{,}5 \pm 0{,}5) \cdot 10^{10}\,\mathrm{M}_\odot$ (Binney and Tremaine, 2008). This disc contains spiral arms, which turn into a bar passing through the disc centre. The bar lies in the galactic plane and extends up to 3 kpc from the galactic centre (Binney and Tremaine, 2008). The disc becomes thicker near its centre, forming the so-called central bulge. The central bulge consists of old stars with randomly oriented orbits. Its mass is estimated to be $M_{\mathrm{bulge}} = (4{,}5 \pm 1{,}5) \cdot 10^9\,\mathrm{M}_\odot$. The rest (and majority) of the galaxy's mass is then located in the halo. Its mass is $M_{\mathrm{halo}} = (2\,^{+3}_{-1{,}8}) \cdot 10^{12}\,\mathrm{M}_\odot$ (Binney and Tremaine (2008)). The halo is a spherical structure around the galactic disc composed mainly of dark matter and globular clusters (dark and stellar halo).

Most of the observed open clusters are located inside the spiral arms, where the gas and dust are compressed, making these regions ideal for star formation. Globular clusters are located in the galactic halo.

2.2 Centre of our galaxy – SgrA*

The centre of our galaxy lies at the constellation Sagittarius, approximately 8300 pc from Earth (Gillessen et al., 2009). The centre of the GC region is considered to be the radio source SgrA*. Its equatorial coordinates in respect to the epoch 2000 are (SIMBAD Astronomical Database – CDS, Strasbourg):

$$\alpha = 17\,h\,45\,\mathrm{min}\,40.03599\,\mathrm{sec} \quad \delta = -29^\circ\,00'\,28.1699'' \tag{2.1}$$

The nature of this object has been the subject of discussions for many years (and it still is). Several stars are observed orbiting this object. Long-term spectroscopic and astrometric observations of those stars have been used to determine their orbital parameters (see for example Gillessen et al., 2009 or Meyer et al., 2012). All stars seem to be moving on Keplerian orbits, suggesting that they are residing in a point-mass potential. The star with the closest aproach to SgrA* (with designation S0-16) has a pericentre distance of only 45 AU (Ghez et al., 2005), and the orbit still remains Keplerian, suggesting that all the mass generating the potential is enclosed within this radius. This mass is estimated to be (Gillessen et al., 2009):

$$M = (4,31 \pm 0,36) \cdot 10^6\,\mathrm{M}_\odot \tag{2.2}$$

This provides the lower constraint for the density of SgrA* to $\sim 9.9 \cdot 10^{16}\,M_\odot/pc^3$ and therefore a strong case for a central supermassive black hole (see for example Ghez et al., 2005 for more detailed discussion).

Gillessen et al. (2009) also determines the distance between Earth and SgrA*:

$$R_0 = (8,33 \pm 0,35)\,\mathrm{kpc} \tag{2.3}$$

2.3 Star clusters in the Galactic Centre

Besides the great amount of gas and free stars (stars spread throughout the field that are not part of any cluster), three star systems are being observed in the GC region: Nuclear star cluster, Arches cluster and the Quintuplet. Their basic properties are going to be described in the following sections.

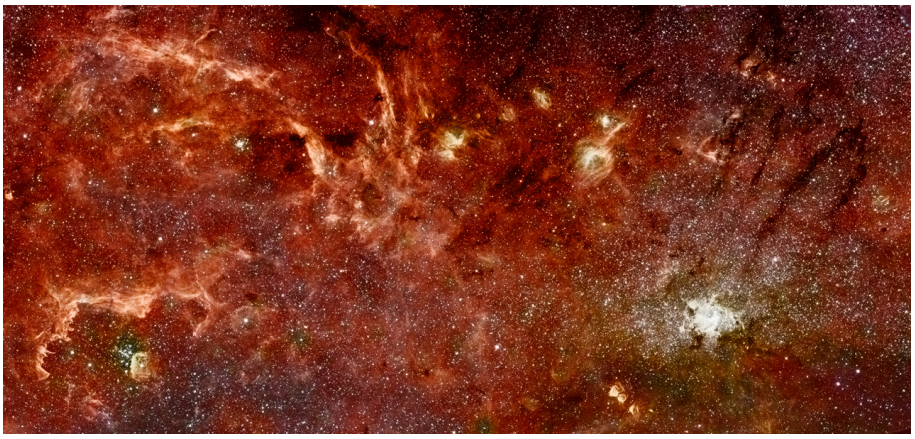

Figure 2.1: Hubble-Spitzer composite of the galactocentric region. At the bottom-right part of the image there is NSC, at the bottom-left there is Quintuplet and the Arches cluster is located at the upper-left part of the image.
Credits: NASA, ESA, Q. D. Wang (University of Massachusetts, Amherst), Jet Propulsion Laboratory, and S. Stolovy (Spitzer Science Center/Caltech)

2.3.1 Nuclear Star Cluster

Nuclear Star Cluster (NSC) directly surrounds the SgrA* object. It is composed of two components – the young and old part of the NSC. The young part of NSC (or Young Nuclear Cluster – YNC) consists of early-type stars with ages of 4-6 Myrs – mainly OB supergiants and W-R stars (see for example Paumard et al., 2006 or Lu et al., 2013). It is confined within the central 0.5 pc of the NSC. The old part of NSC is mainly composed of late-type stars. It reaches several parsecs from the SgrA* object – its half-light radius is ∼5pc (Schödel, 2011).

The YNC can be further divided into the central cusp (within the central 0.05 pc) and outer structures (between 0.05 and 0.5 pc). The outer parts appear to be composed of two warped discs of stars, the so-called "clockwise and counter-clockwise system" (see Bartko et al., 2009 and Genzel et al., 2003). The second disc is, however, not being observed in all studies (see for example Lu et al., 2006 and Lu et al., 2009).

The Young nuclear cluster has undergone extensive studies for many reasons, among others due its closeness to the SgrA* object (it can provide important information about the nature of this object, as discussed in section *2.2*), but also because of its stellar composition. As the name of this part of the NSC already suggests, it is composed of young stars, which is surprising, since the region in the proximity of the central black hole seems to be hostile for classic star formation from gravitationally collapsing clouds (which is how star clusters are normally

born) due to the strong GC potential that tears apart dust clouds located in that region before they start to form the dense and compact fragments from which stars could be potentially born. (Morris, 1993). Several theories have been developed in order to explain the origin of stars in YNC.

Young stars in the central cusp could have been created by collisions of less massive stars (forming so called "blue stragglers"). When two old low-mass stars collide and merge, they can produce one heavy main sequence star, that appears to be young due to its big mass and therefore short life expectancy. The star density in the central 1" allows a sufficient birth rate for such stars (Genzel et al., 2003). Young stars in the outer parts of the cluster have to be explained otherwise. There are two main possible scenarios:

a) **In situ formation** – this scenario supposes that one or more gas clouds fell from the outer parts of the GC and formed a dense disc (or discs) around the central black hole. This disc could have been compressed to the point that it could give birth to new stars even in such a proximity to the central black hole (see Collin and Zahn, 1999).

b) **Cluster infall** – this scenario covers the possibility that the observed disc of stars could have been created by the infall of a pre-existing star cluster (that formed further from the black hole).

The NSC is a complex object composed of several structures most probably of different origins. It is beyond the extent of this thesis to describe all the properties of every one of these parts, since this thesis concentrates mainly on the 'free' clusters moving around the GC with an unknown present-day line-of-sight distance.

2.3.2 Quintuplet

One of the clusters orbiting the GC is called Quintuplet. It was named due to its five brightest stars. Its discovery dates back to 1983 (Kobayashi et al., 1983).

The cluster is located at the projected distance of 32 pc from SgrA*. Its equatorial coordinates for the epoch 2000 are (SIMBAD Astronomical Database – CDS, Strasbourg):

$$\alpha = 17\,h\,46\,\mathrm{min}\,13.9\,\mathrm{sec} \quad \delta = -28^\circ\,49'\,48'' \tag{2.4}$$

Let's define a cartesian coordinate system centered at the GC with x-axis lying in the galactic plane and being perpendicular to the line between Earth and GC, y-axis along the line of sight with positive values in the direction away from Earth and z-axis pointing to the galactic north pole. Then the coordinates of the Quintuplet cluster are as follows:

$$r_{\mathrm{Quintuplet}} = (-28,\, d,\, -2)\,\mathrm{pc} \tag{2.5}$$

Its distance along the line of sight relative to SgrA* (d) is unknown. The galactic centre as a whole is 8 kpc away from Earth where no method for determining distances is precise enough to determine the relative position of the cluster and SgrA*. The exact trajectory of Quintuplet in the galactocentric potential is therefore unknown as well, and so are the effects that this potential can have on the cluster's development.

Its 3D velocity vector has been determined by Stolte et al. (2014) based on spectroscopic and astrometric observations of the cluster. The absolute value of the cluster's velocity is (167 ± 15) km/s in respect to the field, and it is moving almost along the galactic plane. On the sky it is moving away from the galactic centre towards positive galactic longitude, and radially it moves away from Earth. The velocity vector is as follows:

$$v_{\text{Quintuplet}} = (-132,\ 102,\ 0)\,\text{km/s} \tag{2.6}$$

Quintuplet contains a large amount of young heavy stars including W-R stars, OB supergiants and luminous blue variables (Figer et al., 1999b). Its age is estimated to be (4 ± 1) Myrs based on the spectroscopic study of cluster member stars and identifying the main sequence (Figer et al., 1999a) – see section *1.2* for explanation of the method. From newer studies, Lierman et al. (2012) later comes to a similar conclusion.

It is difficult to determine the total mass of the cluster, because only heavy and bright stars can be observed in the GC region. The amount of lighter stars has to be estimated by extrapolating the mass function beyond the observational limits. Hußmann et al. (2012) and Hußmann (2014) determined the total cluster mass to be of the order of $M = 2 \cdot 10^4\,\text{M}_\odot$. They noted that the PDMF is flatter at the centre of the cluster (α = -1.68 at $r < 0.5$ pc) than at its outer parts, where it corresponds to the Salpeter IMF. Mass segregation has therefore taken place in the Quintuplet cluster.

It is worth noting that determining the true IMF of any star cluster in the GC is very difficult due to rapid dynamical evolution of the cluster in the strong GC tidal field. When talking about determining IMF in this context, most authors mean the function of initial masses of stars currently forming the cluster. The difference between PDMF and IMF is therefore in this case only due to stellar evolution and not due to cluster evaporation or tidal stripping, which is hardly traceable.

The origin of the Quintuplet cluster is still unknown. Due to its unknown line-of-sight distance from SgrA*, it is impossible to determine its place of origin. Stolte et al. (2014) performed several simulations of the cluster's movement through a certain GC potential for different present-day line-of-sight distances. They concluded that it is possible that Quintuplet was formed at a transition region between two stable gas-cloud orbits (see Binney et al., 1991), probably by a collision of two gas clouds. If this scenario is correct, then the cluster should now be located in front of the GC, on a prograde orbit.

2.3.3 Arches cluster

The Arches cluster lies at a projected distance of 26 pc (which corresponds to 11' on the sky) from the galactic centre. Its equatorial coordinates for the epoch 2000 are (SIMBAD Astronomical Database – CDS, Strasbourg):

$$\alpha = 17\,h\,45\,\text{min}\,50.5\,\text{sec} \quad \delta = -28^\circ\,49'\,28'' \tag{2.7}$$

Its exact position along the line of sight in respect to the GC is unknown for the same reasons as in the case of Quintuplet. Its position vector in the coordinate

system described in the previous section is:

$$r_{\text{Arches}} = (-23,\, d,\, 8)\,\text{pc} \tag{2.8}$$

where d stands again for the unknown line-of-sight distance from the GC. Since the cluster seems to be interacting with the molecular clouds located in the GC (so-called central molecular zone – CMZ), it is likely that the cluster currently resides in the central 200 pc of the GC region (see Wang et al., 2006; Lang et al., 2003; Stolte et al., 2008). In Stolte et al. (2008) a formation scenario of the Arches cluster is presented, assuming its formation from two colliding gas clouds – the same as for the Quintuplet. If this scenario is correct, the cluster should now be on a prograde orbit and therefore should be located in front of the GC (making d negative). Otherwise the birthplace of the Arches would not fall into the specific GC regions where the collisions of heavy gas clouds are expected (Stolte et al., 2008). Furthermore, the extinction values for the Arches cluster appear to be lower than those of the GC, which gives us another indication that the cluster is currently in front of the GC (see Cotera et al., 1996; Nagata et al., 1995; Stolte et al., 2008).

Unlike the position vector, the velocity vector of the Arches cluster is well known. The radial velocity (along the line of sight) has been determined from sectroscopic data (Figer et al., 2002) to be 95 ± 8 km/s. Proper motion has been derived from astrometric measurements of the cluster during a long period of time yielding two different results: v_{prop} =212 ± 29 (Stolte et al., 2008) and v_{prop} =172 ± 15 km/s (Clarkson et al., 2012), both in the direction parallel to the galactic plane and heading away from the GC as in the case of Quintuplet. The three-dimensional velocity vector of the Arches cluster is then:

$$v_{\text{Arches}} = (-v_{\text{prop}},\, 95,\, 0)\,\text{km/s} \tag{2.9}$$

Like the Quintuplet, Arches also contains many massive stars, mainly W-R stars (5 % of all known stars in the galaxy – Figer et al., 2002) and O-giants (Figer et al., 1999a). The age of the cluster is now estimated to be (2.5 ± 0.5) Myrs (Figer et al., 2002). This result is consistent with several other studies, such as, for example, Martins et al. (2007) or Najarro et al. (2004). The latter studied the stellar metallicity of selected W-R stars and compared it to the theoretical models. They concluded that the age of the cluster should be between 2 and 2.5 Myrs.

The PDMF varies between different authors. Stolte et al. (2002) determined the slope of the PDMF to be α = -1.8 ± 0.2 within the cluster's 0.4 pc radius, which is flatter than the Salpeter IMF. Espinoza et al. (2009) came to the slope of α = -2.1 ± 0.2 within the 0.4 pc and could not discard the Salpeter IMF. Habibi et al. (2013) came to the value of α = -2.53 ± 0.31 within 1.5 pc, which is even steeper than Salpeter, and pointed out that the extinction of the GC environment affects the PDMF/IMF determination significantly. All mentioned authors noticed a mass segregation within the cluster - the cluster centre is dominated by heavy stars and the outskirts by lighter ones. Furthermore, Harfst et al. (2010) performed a set of N-body simulations and concluded that the present state of the Arches cluster can be well explained by the Salpeter IMF. The most recent studies therefore suggest that the centre of the Arches cluster has a flatter mass function than Salpeter IMF, but the overal MF resembles it, and the possibility

that the IMF of the Arches was close to the Salpeter IMF cannot be discarded. The differences between the aforementioned results can be contributed to different field selection (different radii from the cluster centre) but also to problems caused by extinction, which complicate the mass determination of observed stars.

The total mass of the cluster is of order of $10^4\,M_\odot$ (Figer et al., 1999a; Clarkson et al., 2012; Espinoza et al., 2009) and ranges from $1.9 \cdot 10^4$ to $6 \cdot 10^4\,\mathrm{M}_\odot$ between those studies.

2.4 Free stars in the Galactic Centre

Besides the three star clusters present in the GC region, a significant amount of free stars (stars that don't seem to belong to any star cluster) are also observed (Wang et al., 2010; Dong et al., 2011; Mauerhan et al., 2010a; Mauerhan et al., 2010b) – see figure 2.2. These are mostly W-R stars and OB giants. They form about one third of the total stellar population in the GC (Habibi et al., 2014). There are at least four possible explanations for their origin:

1. They could have formed isolatedly from the gas and dust clouds present in the GC region.
2. They could be remnants of an older dissipated cluster (or clusters) formerly present in the GC region.
3. They could have been ejected from the Nuclear Star Cluster.
4. They could have been ejected from the Arches or Quintuplet cluster.

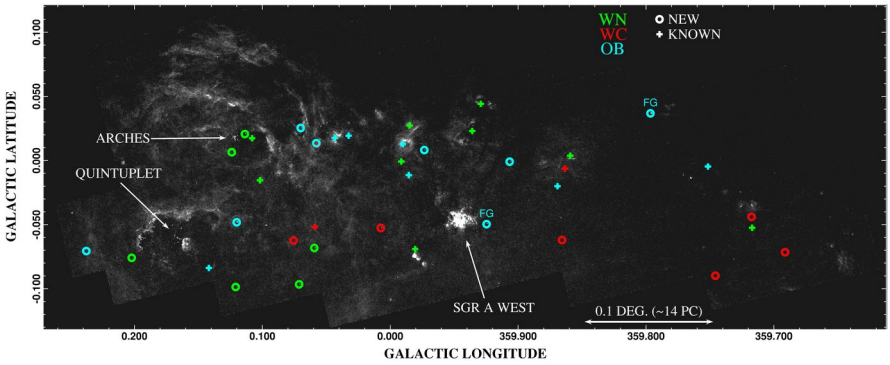

Figure 2.2: Massive isolated stars observed in the GC region. Image taken from Mauerhan et al. (2010a).

Considering option 1, it is not known if massive stars can form isolatedly. Stars are normally formed from a larger dust cloud as a part of a cluster. However it is possible that the conditions in the GC region favor the formation of isolated heavy stars (see Oskinova et al., 2013). The possibility that the free stars in the GC region have formed isolatedly cannot be dismissed.

Another possibility is that those stars were born in some old cluster that no longer exists. However, Figer et al. (2002) argues that the formation of Arches

and Quintuplet clusters was probably unique, since there is no evidence of older clusters (even already dissipated). If the free stars were really remnants of some old cluster, we should see more red supergiants among them, which is not the case (Figer et al., 2002; Figer, 1995).

Concerning option 3, Habibi et al. (2014) argued that the NSC is not expected to produce enough stars to explain the observed GC free star population. Based on the results from Hills (1988); Yu and Tremaine (2003) and Perets et al. (2007) they argue that the interactions between NSC stars and the supermassive black hole should produce high-velocity stars that leave the GC region within 10^4 years and that the ejection rate of such stars is insufficient to produce more than $\sim$1 star observable in the GC region at any given time. This argument only concerns the inner parts of the YNC, where the stars interact with the supermassive black hole. The old part of the NSC doesn't seem to be the main contributor to the free star population, since it is composed of late-type stars and the free stars are mainly young W-R stars and OB giants. What remains is the outer part of the YNC containing the disc-like structure of young stars (see section *2.3.1*). The interactions between stars inside this disc could potentially feed the galactic centre with some amount of young stars. However simulations would be required to estimate the ejection rate from this disc.

The possibility that the free stars have escaped from Arches and Quintuplet clusters is explored by Habibi et al. (2014). They performed several simulations of those two clusters over their supposed lifetimes in a simplified spherically symmetric potential of the GC region and were able to explain 60-80 % of the observed massive stars in the GC region (comparing the results of their simulations with the catalogue provided by Mauerhan et al., 2010a and Mauerhan et al., 2010b). They have chosen only one trajectory for each cluster (corresponding to the present-day line-of-sight distance of -100 pc in the case of the Arches cluster). How the expected contribution of those clusters changes for different trajectries is the main subject of this thesis.

3. Simulations

3.1 Goal

As it is stated in section *2.3.3*, the present-day line-of-sight distance of the Arches cluster from the GC is not known. The aim of the following simulations is to determine how and by how much the amount and spatial distribution of stars escaped from the Arches cluster change for different line-of-sight distances.

Firstly, it is necessary to determine the place of birth of the cluster for each present-day line-of-sight distance. This will be done by simulating the cluster from its current position back for its supposed lifetime (section *3.2*). The cluster will be considered to be a single point (neglecting the internal structure) during those simulations. Once the birth positions are known, a model cluster (see section *3.3* for details) will be simulated (including its internal development) from those points forwards in time for its supposed lifetime. Then the following features are going to be analysed:

1. The percentage of cluster's original mass that will be ejected during its lifetime (section *3.5.1*).
2. The length of its resulting tidal arms (section *3.5.2*).
3. The width of the tidal arms on the plane of the sky (section *3.5.3*).

3.2 Determining Arches' place of birth

I simulated the cluster back in time from its current position for its supposed lifetime of 2.5 Myrs in the GC potential in order to determine its place of birth.

I used the same external potential as was used in the simulations of Habibi et al. (2014). It is a spherical approximation of the GC potential taken from Spinnato et al. (2003). They fitted the observed GC mass distribution from Mezger et al. (1999) with the power-law function:

$$M(r) = (4.25) \cdot 10^6 (\frac{r}{\mathrm{pc}})^{1.2}\,\mathrm{M}_\odot \tag{3.1}$$

This equation does not include the SMBH and therefore is not accurate at the proximities of the GC. In order to correct that I have added the static potential from the SMBH of mass (*2.2*) to my simulations as well. The resulting mass distribution generating the external potential in my simulations is therefore:

$$M(r) = (4.25) \cdot 10^6 (\frac{r}{\mathrm{pc}})^{1.2} + 4.31 \cdot 10^6\,\mathrm{M}_\odot \tag{3.2}$$

I have used the same Arches' current state vector as was used by Habibi et al. (2014) as the starting point:

$$(x,\, y,\, z) = (-24,\, d,\, 10)\,\mathrm{pc}; \quad (v_x,\, v_y,\, v_z) = (-190,\, 95,\, 0)\,\mathrm{km/s} \tag{3.3}$$

where d stands for the unknown present-day line-of-sight distance of the Arches cluster from the galactic centre. The x coordinate goes along the galactic plane, y goes along the line of sight and z goes towards the galactic north pole.

The cluster was considered to be a single point in all these simulations; no internal development was simulated. I used my own integrator that uses a so-called semi-implicit Euler algorithm (see *Appendix*) with a controlled energy error.

For each present-day line-of-sight distance ranging from 0 pc to -200 pc (see section *2.3.3*) with a 20 pc step I determined the place of birth of the cluster. Those initial positions along with the initial velocities are listed in table 3.1, and the corresponding trajectories are rendered in figure 3.1. I have also simulated the cluster forward in time to get the information about its future orbit.

d [pc]	x[pc]	y[pc]	z[pc]	v_x[pc]	v_y[pc]	v_z[pc]
0	8.14	10.74	-12.34	233.18	27.61	-120.17
-20	24.39	-14.45	0.70	-167.46	-150.07	73.06
-40	-18.79	47.37	-7.30	189.72	47.55	-27.39
-60	56.78	-27.54	-0.12	-97.02	-193.87	33.66
-80	-41.07	-74.81	10.36	-196.26	68.12	3.26
-100	-114.26	-24.12	7.25	-43.70	177.02	-13.85
-120	-127.69	41.44	1.70	92.09	166.52	-16.10
-140	-102.66	93.58	-2.78	187.64	110.28	-13.43
-160	-55.78	125.43	-5.67	245.88	32.98	-9.06
-180	1.05	136.24	-7.12	267.37	-51.09	-4.30
-200	58.83	128.44	-7.45	255.41	-127.07	-0.03

Table 3.1: Initial state vectors of the simulated cluster corresponding to different orbits. d is the current line-of-sight distance of the cluster from the GC. The x coordinate goes along the galactic plane, the y along the line of sight and z towards the galactic north pole.

3.3 Initial parameters of the simulated cluster

The IMF, size and mass of the cluster have been taken from Harfst et al. (2010). The authors have performed a set of simulations of a sample cluster in order to find the best initial model of the Arches. They were changing several initial parameters of their cluster, such as the IMF, total mass, concentration and size. After 2.5 Myrs of development they compared the radial density profile, the mass function and the total mass of their sample cluster to the observed properties of the Arches and selected the best fitting model.

The IMF of their best fitting model is the Salpeter IMF, down to the mass of $0.5\,M_\odot$, which I also choose to use in all of my simulations. I also adopt the total initial mass of their best model:

$$M = (4.8) \cdot 10^4\,\mathrm{M}_\odot \tag{3.4}$$

The initial mass distribution of the best fitting model given by Harfst et al. (2010) is a King distribution with a concentration parameter $W_0 = 3$ and a virial radius

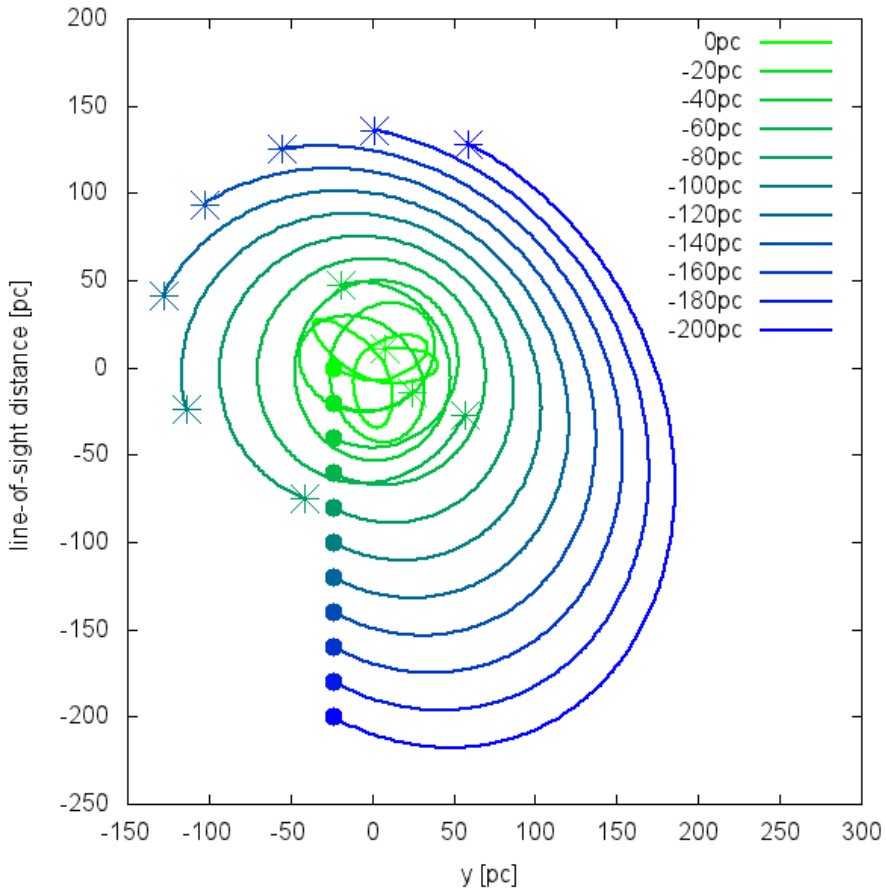

Figure 3.1: Simulated trajectories of the Arches cluster in the GC potential corresponding to different current line-of-sight distances from 0 to -200 pc. The y axis goes along the galactic plane, the x axis goes along the line of sight. The asterisks show the cluster's place of birth and the filled circles its current position.

of $r_{\mathrm{v}} = 0.77\,\mathrm{pc}$. For easier implementation I have chosen a more simple Plummer distribution with a corresponding Plummer scale length:

$$b = r_{\mathrm{v}} \frac{16}{3\pi} \tag{3.5}$$

The orbits of individual stars in Plummer potential are not Keplerian ellipses. However they still have some similar properties; for example, a star moving in a spherically symmetric potential oscillates periodically between minimum and maximum radii from the centre of the potential (apocenter and pericenter distance) as it is in the case of point-mass potential. But the orbits are not necessarily closed. As the first approximation, we can consider stellar orbits in Plummer potential to be Keplerian ellipses that are slowly evolving in time. I have therefore generated stars on initially Keplerian orbits as if they were orbiting around a point of mass equal to the cluster mass enclosed within the radius equal to the semi-major axis (a) of that orbit. The semimajor axes were generated following the Plummer density profile:

$$f(r)\mathrm{d}r = \frac{3}{4\pi b^3}(1 + \frac{r^2}{b^2})^{\frac{5}{2}}\mathrm{d}r \quad F(r) = \frac{r^3}{(r^2 + a^2)^{\frac{3}{2}}} \tag{3.6}$$

where f is the probability density function and F is the cumulative distribution function. Here r has been substituted by the semi-major axis a. This axis is geometrically the average distance of the orbiting body from the centre of mass. Time-averaged distance is, however, different for elliptical orbits, which brings a systematic error to the true resulting cluster mass distribution. I neglected this error for the sake of easier implementation of the algorithm for cluster generation.

Orbit eccentricities were generated following the thermal eccentricity distribution (Jeans, 1919):

$$f(e)\mathrm{d}e = 2e\mathrm{d}e \quad F(e) = e^2 \tag{3.7}$$

This distribution of orbit eccentricities comes from the assumption that the stars are in thermal equilibrium; their kinetic energies follow Bolzmann distribution.

All random variables were generated using a so-called inverse method:

$$x = F^{-1}(w) \tag{3.8}$$

where $F(x)$ is the cumulative distribution function describing the distribution of the desired random variable x and w is a random number from the range 0-1 following a linear distribution.

All the following simulations were performed using the Nbody6 integrator created by Sveere Aarseth (Aarseth, 2003).

3.4 Determining escaped stars

In order to describe the degree of dissipation of my simulated clusters (section *3.5.1*) I need to determine which stars are still part of the cluster and which ones are already free. For that reason I calculated the cluster's Hill sphere - the radius at which the external potential starts to have more effects on the individual stars than the potential of the cluster itself. Assuming that the cluster is on an elliptical orbit, the radius of the Hill sphere is as follows (Hamilton and Burns, 1992):

$$r_{\mathrm{Hill}} \approx a(1-e)\sqrt[3]{\frac{m}{3M}} \tag{3.9}$$

where a is the semi-major axis of the cluster's orbit, e is the eccentricity of that orbit, m is the cluster's mass and M is the mass of the GC, assuming that all its mass is concentrated in one central point. The GC potential is of course not a point-mass potential, and the cluster's trajectory is not elliptical. However the GC potential is spherically symmetric, so at any given position, the cluster experiences forces only from the GC mass enclosed within the sphere of the radius equal to the cluster-GC distance (R), as it would if all this mass were concentrated in one central point. Based on the momentary velocity and position vector of the cluster (centre of mass of stars within 5 pc from the cluster's expected position – (2.8)), I calculate the parameters of its elliptical orbit around that point of mass. I then use the resulting semi-major axis and eccentricity in the above equation.

However, since the cluster is not a single point, the mass m is dependent on r_{Hill}, so I still cannot use the equation as it is. For simplification I assume that the cluster is spherically symmetric. The mass m is then the mass of all stars

located under the Hill radius. Even M is dependent on r_{Hill}, since it is the GC mass enclosed within the radius $R - r_{\mathrm{Hill}}$. The equation (3.9) can be rewritten as follows:

$$r_{\mathrm{Hill}} \approx a(1-e)\sqrt[3]{\frac{m(r_{\mathrm{Hill}})}{3M(R-r_{\mathrm{Hill}})}} \tag{3.10}$$

In order to determine r_{Hill} I wrote an iterative procedure that calculated m and M for a set of radii r_{prob} (which were substituted for r_{Hill} at the right side of the equation) from 0.01 to 20 pc with a step of 0.01 pc. With that m and M the equation (3.9) was used to determine r_{Hill}. The resulting Hill radius of the cluster was taken from the iteration of minimal difference between r_{Hill} and r_{prob}.

3.5 Results

I generated random clusters with initial parameters described in section *3.3* and placed them at the calculated points of origin (table 3.1). I then simulated their development for approximately 2.5 Myrs (the estimated age of the Arches cluster) and studied the cluster's degree of dissipation and the spatial distribution of the escaped stars. I performed three realizations for each trajectory to get an idea of how much the results differ between different realizations. The output quantities from the following sections are mean values from those realizations, and the errors are estimates of the standard deviation of the mean based on Student's distribution.

3.5.1 Degree of dissipation

First I look at the degree of dissipation of the cluster, more specifically at the percentage of mass of stars located outside the cluster's Hill sphere after 2.5 Myrs of the cluster's development (present state). I calculated the radii of the Hill sphere separately for every simulated cluster using the method described in section *3.4*. Then I have averaged the results of clusters on the same orbit. The resulting radii are listed in table 3.2. The average percentages of ejected mass (p_{diss}) for each trajectory are listed in table 3.3. The ejected masses in solar units are also listed in table 3.3.

As can be seen, on the innermost orbit (corresponding to the line-of-sight distance of 0 pc) the cluster is completely dissipated in all realizations. The dissipation decreases very rapidly with a growing line-of-sight distance up to the orbit of $d \approx$-60 pc. Then the dependence becomes flatter until it's practically constant for $d <$-120 pc, where the dissipation reaches only $\approx$23 %. This result alone already makes the innermost orbit highly improbable, since the remaining cluster would be practically non-existent and yet it is observed on the sky.

d [pc]	$r_{\rm Hill}$ [pc]	$\sigma_{r\rm Hill}$ [pc]
0	0.01	0.02
-20	0.58	0.01
-40	1.29	0.02
-60	1.64	0.01
-80	1.7	0.01
-100	1.73	0.01
-120	1.77	0.01
-140	1.81	0.01
-160	1.85	0.01
-180	1.89	0.01
-200	1.93	0.01

Table 3.2: Hill sphere radii ($r_{\rm Hill}$) of the simulated cluster at different present-day line-of-sight distances. The listed radii are mean values of the three realizations of each orbit. σ_r stands for standard deviation.

Habibi et al. (2014) reported that their best model of the Arches and Quintuplet clusters reproduced 60-80 % of observed isolated stars. In their model, the Arches cluster was located at d =-100 pc. As can be seen from my simulations, clusters on orbits of d >-100 pc are significantly more dissipated. For example, the cluster on orbit of d=-40 pc produces 69% more stars than the one on the orbit of -100 pc. Placing the Arches cluster on orbits closer to the GC (d >-100 pc) could therefore possibly reproduce more of the isolated stars than 60-80 %.

d [pc]	$p_{\rm diss}$[%]	$\sigma_{p\rm diss}$[%]	$M_{\rm ej}[10^3 \cdot M_\odot]$	$\sigma_{M\rm ej}[10^3 \cdot M_\odot]$
0	100	0	48	0
-20	85	8	41	4
-40	45	1	21.5	0.6
-60	31.9	0.9	15.3	0.4
-80	27.9	0.8	13.4	0.4
-100	26	1	12.7	0.5
-120	24.6	0.2	11.8	0.1
-140	24	1	11.6	0.5
-160	22.7	0.4	10.9	0.2
-180	23	1	10.9	0.5
-200	22.7	0.4	10.9	0.2

Table 3.3: Percentage of cluster mass located outside the cluster tidal radius after 2.5 Myrs for each simulated orbit ($p_{\rm diss}$). This mass is listed in column $M_{\rm ej}$, σ stands for standard deviation.

3.5.2 Length of tidal arms

In this section I determine and compare the length of tidal arms of the simulated cluster on different orbits. I project each star perpendicularly on the cluster's orbit and then calculate the distance of this projected point from the current position of the centre of the simulated cluster (see figure 3.2).

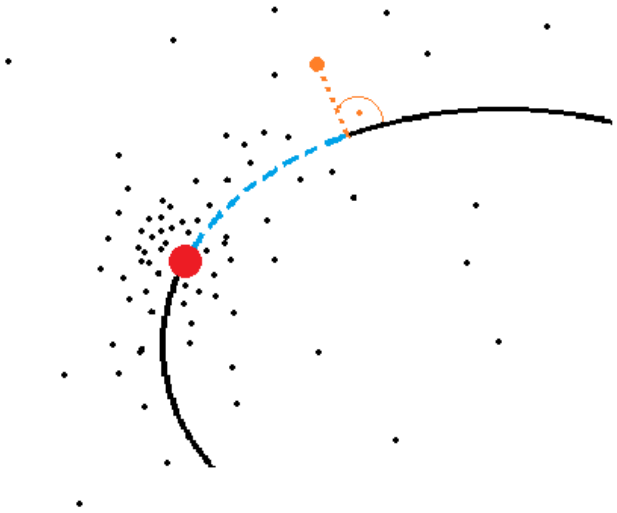

Figure 3.2: Calculating the star's distance from the cluster along the cluster's trajectory (schema). Big red circle is the centre of the simulated cluster, small orange circle is the selected star and the dashed blue line is the resulting distance.

I then constructed histograms showing the one-dimensional distribution of simulated stars along the cluster's orbit. Each bin represents the number of stars that are projected to the corresponding part of the orbit (see schema 3.2). Each bin in these histograms shows the mean value from my realizations. Example histograms for different line-of-sight distances are shown in figure 3.4.

d [pc]	a_t [pc]	σ_{at} [pc]	a_l [pc]	σ_{al} [pc]	b_t [pc]	σ_{bt} [pc]	b_l [pc]	σ_{bl} [pc]
0	83	5	43	2	77	1	38	3
-20	71	3	54	1	71	1	21	1
-40	45	1	46	2	47	2	25	1
-60	39	1	43	4	39	1	31	1
-80	34	2	35	2	31	1	26	1
-100	31	2	33	2	29	2	24	1
-120	31	3	35	1	27	1	25	2
-140	31	1	29	2	28	1	24	3
-160	27	2	28	1	25	2	23	2
-180	27	2	26	4	23	2	23	2
-200	25	4	24	2	23	2	23	4

Table 3.4: Lengths of tidal arms for simulated clusters on different orbits. a_l is the length of the leading arm and a_t of the trailing arm, both in the 3D space. b_l and b_t are lengths of those arms when projected on the plane of the sky. The errors have been calculated by the formula 3.11.

At first look, the distributions of stars are symmetrical except in the case of the innermost orbit (d =0 pc). For orbits corresponding to line-of-sight distances between -20 and -80 pc, each arm (leading and trailing) exhibits a peak in the one-dimensional stellar density. The positions of those peaks are listed in table

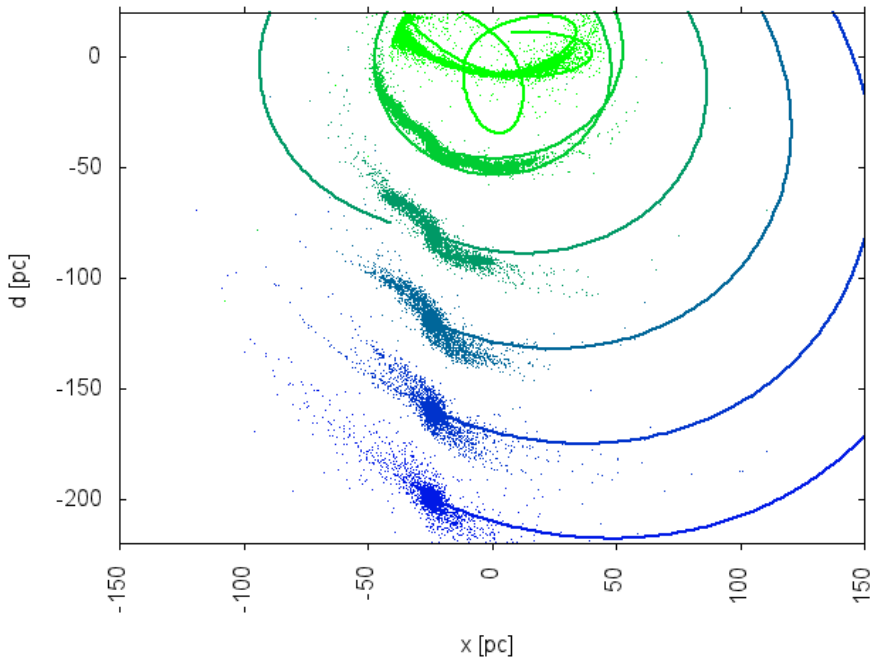

Figure 3.3: Simulated clusters after 2.5 Myrs of development on different orbits viewed from above the galactic plane (which is similar to the cluster's orbital plane). The axis labeled d is the line-of-sight distance. The curves represent clusters' past orbits. As can be seen, the leading arms are closer to the GC while bacwards arms are above the orbit of the cluster itself (see section 1.3.4).

3.5 in section *3.5.3*. At larger orbits no peaks are present; the stellar number-density declines steadily with increasing distance from the cluster.

In order to determine the length of tidal arms from the histograms described above, a fixed one-dimensional stellar number-density has been chosen to depict the edge of the arm. Analyzing the parts of the histograms far beyond the tidal arms, it could be seen that the stellar number-density in those regions tend not to exceed 2 stars per parsec. In order to eliminate the effect of random fluctuations I define the edge of the tidal arm as the point at which the one-dimensional stellar number-density drops below 5 stars per parsec. The resulting lengths of both leading and trailing tidal arms (a_l and a_t respectively) for clusters on different trajectories are listed in table 3.4. The errors have been calculated using the following formula:

$$\sigma = \sqrt{b^2 + \sigma_r^2} \tag{3.11}$$

where b is the size of the bin (1 pc) and σ_r is the estimate of the standard deviation based on the results of different realizations.

The dependence of the length of tidal arms on d is strong in the case of inner orbits. The arm lengths range from 83 to 39 pc for the orbits below -60 pc, but only 33-24 pc for the orbits of d <-100 pc. This could be expected because the gradient of the external potential is highest at the proximities of the GC. The tidal arms are symmetrical in length in the case of orbits of d <-40. In the case of inner orbits, the arms are asymmetrical – the trailing arm becomes larger than the leading one.

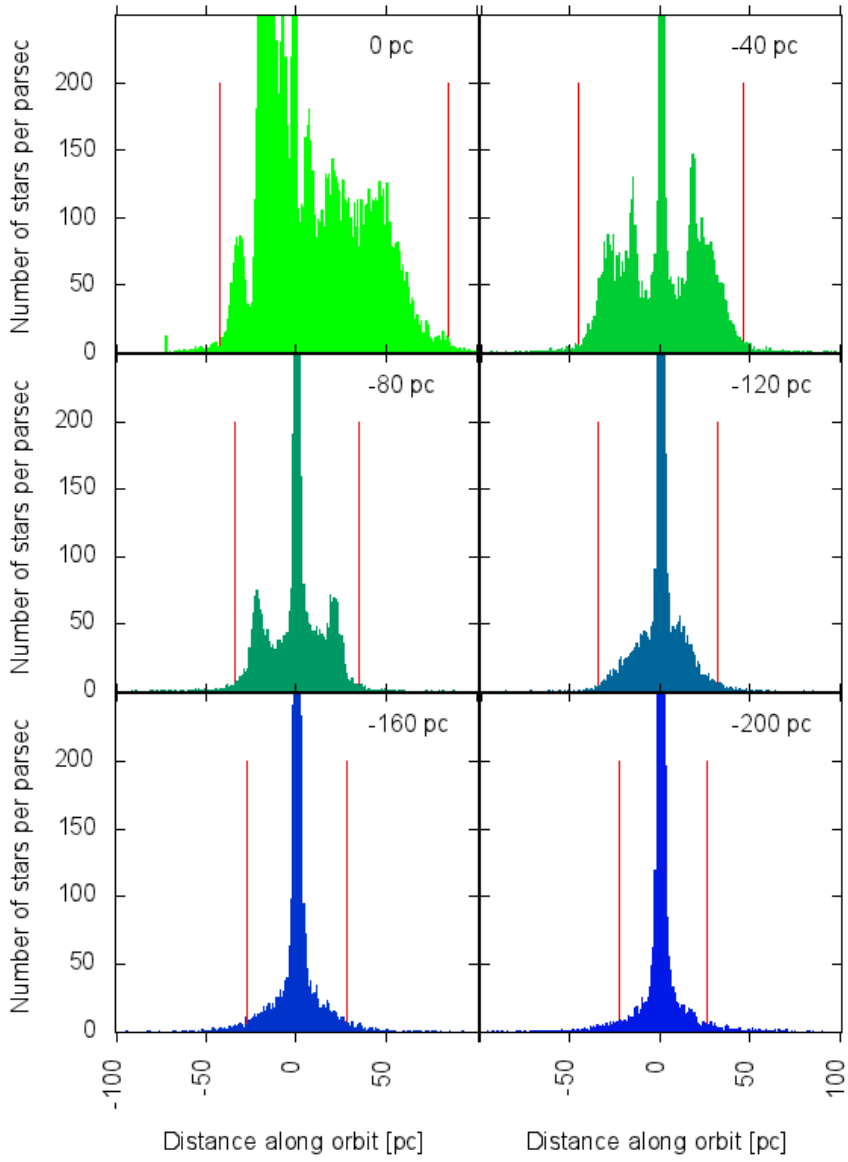

Figure 3.4: Distribution of stars along the cluster's future and past orbit (negative and positive values on the horizontal axis respectively). The height of a bin represents the number of stars projected to the corresponding orbit parsec. The red lines represent the calculated edges of cluster's tidal arms, which are listed in table 3.4. Negative/positive values on the horizontal axis corresponds to the cluster's leading/trailing arm.

I also determined the lengths of the arms on the plane of the sky (b_l and b_t for leading and trailing arm). They are listed in table 3.4 along with a_l and a_t. The projected arms are smaller compared to their 3D length and they are asymmetrical for inner orbits up to d=-100 pc.

Habibi et al. (2014) reported that their best model of the Arches cluster (on d=-100 pc) produced tidal arms reaching up to 20 pc from the cluster in both directions on the plane of the sky. From my simulations it comes out that the length of those arms would not dramatically change if the cluster would have been simulated on outer orbits of d <-100 pc. The length of the arms starts to grow

rapidly in the case of inner orbits ($d > \approx$-80 pc). Habibi et al. (2014) stated that their model is capable of reproduce 80 % of observed stars in the 20 pc neighbourhood of the Arches cluster and 60 % of stars in the 80 pc radius. Placing the cluster on lower orbits would predict longer tidal arms and could therefore explain more stars up to greater distances from the Arches.

3.5.3 Width of tidal arms projected on the plane of the sky

In this section I study how far the stars forming tidal arms are located from the cluster's past and future orbit, e.g. the concentration of the trails of stars which the cluster produces on different orbits. As can be seen from figures 3.3 and 3.5, the situation will be different when considering the distances in the galactic plane vs. the distances projected on the plane of the sky. In the view from above the galactic plane (3.3) (which is very similar to the orbital plane of the cluster) it can be seen that the two arms are systematically shifted from the cluster's orbit. This phenomena is discussed in section *1.3.4*. This feature is not going to be observable from Earth (we are looking at the cluster's orbit plane from the side, not from above), so I am more interested in the situation projected on the plane of the sky. I study the tidal arms up to their lengths calculated in the previous section, and for each orbit parsec I calculate the mean distance (on the plane of the sky) of stars that are projected to that orbit section from the orbit (dotted orange line in schema 3.2). In the following text I will refer to this quantity as the spread of the arms. The results are shown in figure 3.6.

The arms' spread generally grows with the distance from the cluster. It does not exceed 10 pc within the arms' range for any trajectory.

d [pc]	q_t [pc]	q_l [pc]	s_t [pc]	s_l [pc]
-20	15	10	-	-
-40	20	15	-	-
-60	23	19	22	20
-80	24	22	24	23

Table 3.5: Approximate distances of peaks in the one-dimensional stellar density of the trailing and leading arm from the cluster's centre (q_t and q_l respectively) along with distances of local minimas of spreads of the arms from the centre of the cluster (s_t and s_l). The minimas of spreads are not present for orbits of d=-20 pc and d=-40 pc.

For orbits corresponding to line-of-sight distances between -60 and -80 pc, some local minimas are present in the graphs. They correspond with the local maximas in the histograms in figure 3.4. Distances of both local extremes from the centre of the cluster are listed in table 3.5. It appears that the peaks in the one-dimensional stellar density (see previous section) correspond to thinner parts of the arm. There is also an asymmetry between the leading and trailing arm in the case of all orbits except the outermost one – the spread of the leading arm seems to grow more rapidly than that of the trailing arm.

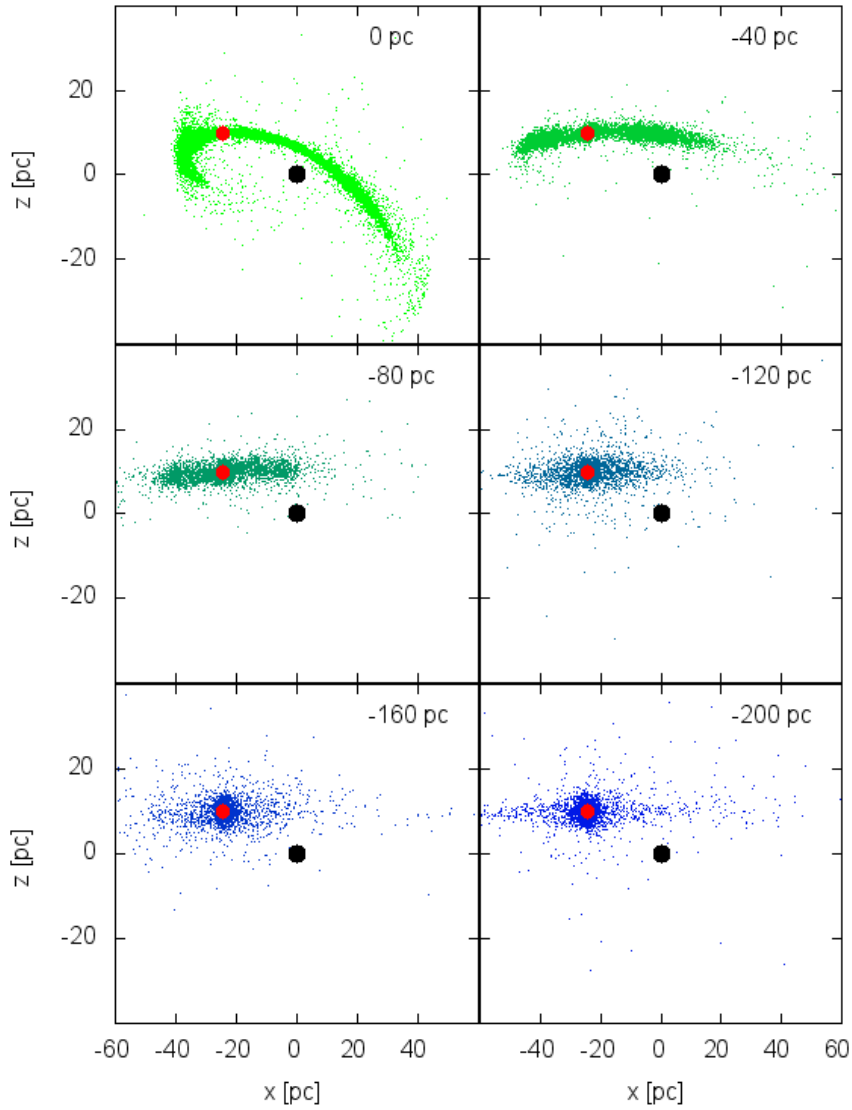

Figure 3.5: Simulated clusters after 2.5 Myrs of development on different orbits projected on the plane of the sky. The x axis goes along the galactic plane. The black circle at the centre is the SgrA object and the red circle shows the current position of the cluster.*

I also calculated the mean distances of stars from the orbit as a whole (not parsec by parsec) – e.g. mean spreads of the arms (m_t and m_l for trailing and leading arm). They are listed in table 3.6 separately for the trailing and leading arm. Those mean spreads were calculated from the stars located within the range of the tidal arms; that means that their distance from the cluster along the cluster's orbit (dashed blue curve in schema 3.2) is lower than the corresponding length of the tidal arm calculated in the previous section and greater than the cluster's Hill sphere radius calculated in section *3.4*. The resulting mean spreads range from approximately 1.2 pc to 3.6 pc. They generally grow with the line-of-sight distance, especially in the range -40> d >-120 pc. For the innermost orbits and outermost orbits this growth is practically null. As can be already expected

from the spread profiles (figure 3.6), the leading arm has a higher mean spread than the trailing arm in all cases except the two outermost orbits (in those cases it can be due to the statistical errors). The relative differences between m_t and m_l are higher for the inner orbits – m_l is up to 2 times greater than m_t.

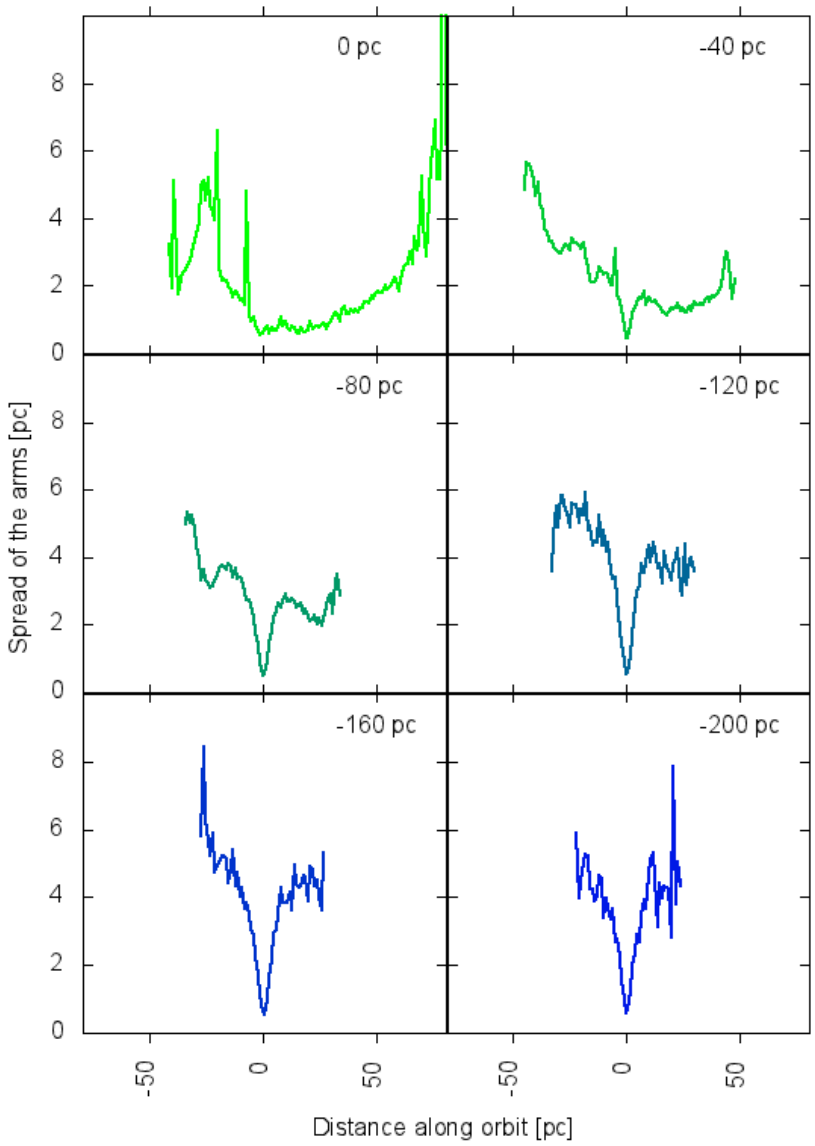

Figure 3.6: Mean separation of stars from the cluster's orbit on the plane of the sky (spread of the arms) as a function of distance along the orbit from the centre of the cluster. Each figure corresponds to one orbit. Negative values on the horizontal axis correspond to cluster's future orbit (and leading arm), positive values to past orbit (trailing arm).

Simulations of Habibi et al. (2014) produced two strips of stars on the sky – one created by the Arches cluster and the second by the Quintuplet. They argued that it is similar to what is observed on the plane of the sky (Mauerhan et al., 2010a). As can be seen, all of my simulations produced a relatively concentrated strip of stars on the plane of the sky as well. The differences between orbits are

not very significant when considering the with of arms on the plane of the sky. Differences in their length are much more prominent

d [pc]	m_{t} [pc]	$\sigma_{m\mathrm{t}}$ [pc]	m_{l} [pc]	$\sigma_{m\mathrm{l}}$ [pc]
0	1.28	0.07	2.2	0.2
-20	1.26	0.04	2.7	0.07
-40	1.33	0.01	2.5	0.1
-60	1.73	0.01	2.86	0.08
-80	2.3	0.02	3.01	0.07
-100	2.94	0.04	3.4	0.1
-120	3.3	0.1	3.59	0.05
-140	3.26	0.04	3.53	0.02
-160	3.09	0.04	3.4	0.1
-180	2.98	0.01	2.9	0.2
-200	3.1	0.2	2.7	0.2

Table 3.6: Average distances of stars from the cluster's orbit when projected on the plane of the sky (mean spreads of the arms). m_t and m_l correspond to the cluster's trailing and leading arm respectively. These values represent the average widths of individual arms.

4. Conclusions

I performed a set of N-body simulations of the Arches cluster in the galactic centre for different present-day line-of-sight distances (d) ranging from 0 to -200 pc. I studied how much the degree of dissipation of the cluster and extents of its tidal arms depend on this unknown variable.

Choosing the present-day line-of-sight distance of the Arches cluster as the end point of the simulations can result in different amounts and spatial distributions of escaped stars and therefore change what percentage of observed stars can or cannot be explained as the Arches-escapers.

The tidal arms on inner orbits (d >-100 pc) are thinner (1.26-3 pc), contain bigger portion of Arches' stars (28-100%) and reach further from the centre of the cluster (34-83 pc). They can therefore explain more of the observed free GC stars and to greater distances from Arches' current position. On the orbits of -20> d >-80 pc the tidal arms show a specific structure – peaks in the stellar density located at 15-24 pc from the cluster's position. At those points the arms are also thinner than at other parts. With improving observational techniques capable of detecting more free GC stars, it could be possible to look for those structures around the Arches' orbit and put more constraints on the cluster's line-of-sight distance. The orbit of d=0 pc results to be highly improbable, since the simulated cluster was completely disintegrated and therefore should not be observable on the sky.

Outer orbits produce distributions of free stars that are much more similar to each other than in the case of inner orbits. The tidal arms are less dense (contain smaller portion of Arches' stars – 23-26 %) and their edges are not as sharp. They reach only to 24-35 pc from the cluster and are thicker (2.7-3.6 pc). They can explain fewer free GC stars, leaving place for other theories about their origin.

Habibi et al. (2014) reported that their best model of the Arches and Quintuplet clusters reproduced up to 80 % of observed stars in the 20 pc radius from the Arches cluster and 60 % of stars in the 80 pc radius. This could be partially resolved by placing the cluster closer to the GC (d >-100). Let's consider, for example, the orbit of d=-40 pc The cluster from my simulations on that orbit produces 69% more stars than the one on the orbit of -100 pc. The trailing arm of the cluster on the orbit of d=-40 pc also reaches to larger distances from the cluster on the plane of the sky – by approximately 20 pc than it does in the case of d=-100 pc. Placing the cluster closer to the GC could therefore potentially further improve the results of Habibi et al. (2014) by explaining more observed isolated stars and up to greater distances from the cluster.

5. Appendix – Semi-implicit Euler method of integration

The so called semi-implicit Euler method is a relatively simple integrator which can be used for simulation of N-body systems. It works as follows: Let x_{in} and v_{in} be the position and velocity of the i-th particle from an N-body system at the n-th iteration of the algorithm (at time t_n). Then the position and velocity of that particle in the iteration n+1 (at time $t_{(n+1)}$) is:

$$v_{i(n+1)} = v_{in} + a_{in}\Delta t \tag{5.1}$$

$$x_{i(n+1)} = x_{in} + v_{i(n+1)}\Delta t \tag{5.2}$$

where a_{in} is the acceleration of the i-th particle at time t_n (caused by other particles and other external forces) and Δt is the simulation step.

Although this method almost preserves the total energy of the system (see Hairer et al. (2003) for more detailed analysis), I have implemented this method along with an energy checker. For each step it calculates the potential and kinetic energy of all particles (only one particle in the case of my simulations) and registers its deviation from the original total energy of the system (at step 0):

$$E_{\mathrm{err}} = \frac{\sum_{i=1}^{N} E_{in} - \sum_{i=1}^{N} E_{i0}}{\sum_{i=1}^{N} E_{i0}} \tag{5.3}$$

where E_{in} is the sum of potential and kinetic energy of the i-th particle at the n-th iteration of the algorithm.

Bibliography

S. Aarseth. *Gravitational N-Body Simulations*. Cambridge Monographs on Mathematical Physics. Cambridge University Press, 2003. ISBN 9780511535246.

H. Bartko, F. Martins, T. K. Fritz, et al. Evidence for Warped Disks of Young Stars in the Galactic Center. *The Astrophysical Journal*, 697:1741–1763, 2009. ISSN 0004-637X.

N. Bastian, K. R. Covey, and M. R. Meyer. A Universal Stellar Initial Mass Function? A Critical Look at Variations. *Annual Review of Astronomy and Astrophysics*, 48:339–389, 2010. ISSN 0066-4146.

J. Binney and S. Tremaine. *Galactic Dynamics*. Second Edition. Princeton University Press, New Jersey, 2008. ISBN 9780691130279.

J. Binney, O. E. Gerhard, A. A. Stark, et al. Understanding the kinematics of Galactic centre gas. *Monthly Notices of the Royal Astronomical Society*, 252: 210–218, 1991. ISSN 0035-8711.

T. Böker. Nuclear star clusters. *Proceedings of the International Astronomical Union*, 266:58–63, 2010. ISSN 1743-9213.

CDS, Strasbourg. SIMBAD Astronomical Database. `http://simbad.u-strasbg.fr/simbad/`. Last accessed 17. June 2017.

W. I. Clarkson, A. M. Ghez, M. R. Morris, et al. Proper Motions of the Arches Cluster with Keck Kaser Guide Star Adaptive Optics: The First Kinematic Mass Measurement of the Arches. *The Astrophysical Journal*, 751:132–165, 2012. ISSN 0004-637X.

S. Collin and J.-P. Zahn. Star formation and evolution in accretion disks around massive black holes. *Astronomy and Astrophysics*, 344:433–449, 1999. ISSN 0004-6361.

A. S. Cotera, E. F. Erickson, S. W. J. Colgan, et al. The Discovery of Hot Stars near the Galactic Center Thermal Radio Filaments. *The Astrophysical Journal*, 461:750–761, 1996. ISSN 0004-637X.

H. Dong, Q. D. Wang, A. Cotera, et al. Hubble Space Telescope Paschen α survey of the Galactic Centre: data reduction and products. *Monthly Notices of the Royal Astronomical Society*, 417:114–135, 2011. ISSN 0035-8711.

P. Espinoza, F. J. Selman, and J. Melnick. The massive star initial mass function of the Arches cluster. *Astronomy and Astrophysics*, 501:563–583, 2009. ISSN 0004-6361.

D. F. Figer. A Search for Emission-Line Stars Near the Galactic Center. *PhDT*, 1995.

D. F. Figer, S. S. Kim, M. Morris, et al. Hubble Space Telescope/NICMOS Observations of Massive Stellar Clusters near the Galactic Center. *The Astrophysical Journal*, 525:750–758, 1999a. ISSN 0004-637X.

D. F. Figer, I. S. McLean, and M. Morris. Massive Stars in the Quintuplet Cluster. *The Astrophysical Journal*, 514:202–220, 1999b. ISSN 0004-637X.

D. F. Figer, F. Najarro, D. Gilmore, et al. Massive Stars in the Arches Cluster. *The Astrophysical Journal*, 581:258–275, 2002. ISSN 0004-637X.

R. Genzel, R. Schödel, T. Ott, et al. The Stellar Cusp around the Supermassive Black Hole in the Galactic Center. *The Astrophysical Journal*, 594:812–832, 2003. ISSN 0004-637X.

A. M. Ghez, S. Salim, S. D. Hornstein, et al. Stellar Orbits around the Galactic Center Black Hole. *The Astrophysical Journal*, 620:744–757, 2005. ISSN 0004-637X.

S. Gillessen, F. Eisenhauer, S. Trippe, et al. Monitoring Stellar Orbits Around the Massive Black Hole in the Galactic Center. *The Astrophysical Journal*, 692: 1075–1109, 2009. ISSN 0004-637X.

M. Habibi, A. Stolte, W. Brandner, et al. The Arches cluster out to its tidal radius: dynamical mass segregation and the effect of the extinction law on the stellar mass function. *Astronomy and Astrophysics*, 556:A26, 2013. ISSN 0004-6361.

M. Habibi, A. Stolte, and S. Harfst. Isolated massive stars in the Galactic center: The dynamic contribution from the Arches and Quintuplet star clusters. *Astronomy and Astrophysics*, 566:A6, 2014. ISSN 0004-6361.

E. Hairer, Ch. Lubich, and G. Wanner. Geometric numerical integration illustrated by the Störmer/Verlet method. *Acta Numerica*, 12:399–450, 2003. ISSN 0962-4929.

D. P. Hamilton and J. A. Burns. Orbital stability zones about asteroids. II - The destabilizing effects of eccentric orbits and of solar radiation. *Icarus*, 96:43–64, 1992. ISSN 0019-1035.

S. Harfst, S. P. Zwart, and A. Stolte. Reconstructing the Arches cluster – I. Constraining the initial conditions. *Monthly Notices of the Royal Astronomical Society*, 409:628–638, 2010. ISSN 0035-8711.

J. G. Hills. Hyper-velocity and tidal stars from binaries disrupted by a massive Galactic black hole. *Nature*, 331:687–689, 1988. ISSN 0028-0836.

B. Hußmann. The Quintuplet cluster - A young massive cluster study based on proper motion membership. *PhD Thesis*, 2014.

B. Hußmann, A. Stolte, W. Brandner, et al. The present-day mass function of the Quintuplet cluster based on proper motion membership. *Astronomy and Astrophysics*, 540:A57, 2012. ISSN 0004-6361.

J. H. Jeans. The origin of binary systems. *Monthly Notices of the Royal Astronomical Society*, 79:408–416, 1919. ISSN 0035-8711.

Y. Kobayashi, H. Okuda, S. Sato, et al. nfrared polarization in the direction to the galactic center. *Astronomical Society of Japan, Publications*, 35:101–112, 1983. ISSN 0004-6264.

C. C. Lang, K. E. Johnson, W. M. Gross, et al. Multifrequency Radio Observations of the Galactic Center Quintuplet and Arches Clusters. *Bulletin of the American Astronomical Society*, add volume:add pages, 2003. ISSN 0002-7537.

A. Lierman, W. R. Hamann, L. M. Oskinova, et al. The Quintuplet cluster. III. Hertzsprung-Russell diagram and cluster age. *Astronomy and Astrophysics*, 540:A14, 2012. ISSN 0004-6361.

J. R. Lu, A. M. Ghez, S. D. Hornstein, et al. Galactic Center Youth: Orbits and Origins of the Young Stars in the Central Parsec. *Journal of Physics: Conference Series*, 54:279–287, 2006. ISSN 1742-6588.

J. R. Lu, A. M. Ghez, S. D. Hornstein, et al. A Disk of Young Stars at the Galactic Center as Determined by Individual Stellar Orbits. *The Astrophysical Journal*, 690:1463–1487, 2009. ISSN 0004-637X.

J. R. Lu, T. Do, A. M. Ghez, et al. Stellar Populations in the Central 0.5 pc of the Galaxy. ii. The Initial Mass Function. *The Astrophysical Journal*, 764: 155–171, 2013. ISSN 0004-637X.

F. Martins, D. J. Hillier, T. Paumard, et al. The most massive stars in the Arches cluster. *Astronomy and Astrophysics*, 478:219–233, 2007. ISSN 0004-6361.

J. C. Mauerhan, A. Cotera, H. Dong, et al. Isolated Wolf-Rayet Stars and O Supergiants in the Galactic Center Region Identified Via Paschen-α Excess. *The Astrophysical Journal*, 725:188–199, 2010a. ISSN 0004-637X.

J. C. Mauerhan, M. P. Muno, M. R. Morris, et al. Near-infrared Counterparts to Chandra X-ray Sources Toward the Galactic Center. II. Discovery of Wolf-Rayet Stars and O Supergiants. *The Astrophysical Journal*, 710:706–728, 2010b. ISSN 0004-637X.

L. Meyer, A. M. Ghez, R. Schödel, et al. The Shortest-Known-Period Star Orbiting Our Galaxy's Supermassive Black Hole. *Science*, 338:84–87, 2012. ISSN 0036-8075.

P. G. Mezger, R. Zylka, S. Philipp, and R. Launhardt. The nuclear bulge of the Galaxy. II. The K band luminosity function of the central 30 PC. *Astronomy and Astrophysics*, 348:457–465, 1999. ISSN 0004-6361.

M. Morris. Massive star formation near the Galactic center and the fate of stellar remnants. *The Astrophysical Journal*, 408:496–506, 1993. ISSN 0004-637X.

T. Nagata, Ch. E. Woodward, M. Shure, et al. Object 17: Another cluster of emission-line stars near the galactic center. *Astronomical Journal*, 109:1676–1681, 1995. ISSN 0004-6256.

F. Najarro, D. F. Figer, D. Hillier, et al. Metallicity in the Galactic Center: The Aarches Cluster. *The Astrophysical Journal*, 611:105–108, 2004. ISSN 0004-637X.

Nilakshi, R. Sagar, A. K. Pandey, and V. Mohan. A study of spatial structure of galactic open star clusters. *Astronomy and Astrophysics*, 183:153–162, 2002. ISSN 0004-6361.

L. M. Oskinova, M. Steinke, W. R. Hamann, et al. One of the most massive stars in the Galaxy may have formed in isolation. *Monthly Notices of the Royal Astronomical Society*, 436:add pages, 2013. ISSN 0035-8711.

T. Paumard, R. Genzel, F. Martins, et al. The Two Young Star Disks in the Central Parsec of the Galaxy: Properties, Dynamics, and Formation. *The Astrophysical Journal*, 643:1011–1035, 2006. ISSN 0004-637X.

H. B. Perets, C. Hopman, and T. Alexander. Massive Perturber-driven Interactions between Stars and a Massive Black Hole. *The Astrophysical Journal*, 669: 709–720, 2007. ISSN 0004-637X.

H. C. Plummer. On the problem of distribution in globular star clusters. *Monthly Notices of the Royal Astronomical Society*, 71:460–470, 1911. ISSN 0035-8711.

E. E. Salpeter. The Luminosity Function and Stellar Evolution. *The Astrophysical Journal*, 121:161–167, 1955. ISSN 0004-637X.

R. Schödel. The Milky Way Nuclear Star Cluster in Context. *Astronomical Society of the Pacific Conference Series*, 439:222–231, 2011.

P. F. Spinnato, M. Fellhauer, and Z. Portegies. The efficiency of the spiral-in of a black hole to the Galactic Centre. *Monthly Notices of the Royal Astronomical Society*, 344:22–32, 2003. ISSN 0035-8711.

A. Stolte, E. K. Grebel, W. Brandner, et al. The mass function of the Arches cluster from Gemini adaptive optics data. *Astronomy and Astrophysics*, 394: 459–478, 2002. ISSN 0004-6361.

A. Stolte, A. M. Ghez, M. Morris, et al. The Proper Motion of the Arches Cluster with Keck Laser-Guide Star Adaptive Optics. *The Astrophysical Journal*, 675: 1278–1292, 2008. ISSN 0004-637X.

A. Stolte, B. Hußmann, M. R. Morris, et al. The Orbital Motion of the Quintuplet Cluster - A Common Origin for the Arches and Quintuplet Clusters? *The Astrophysical Journal*, 789:115–135, 2014. ISSN 0004-637X.

Q. D. Wang, H. Dong, and C. Lang. The interplay between star formation and the nuclear environment of our Galaxy: deep X-ray observations of the Galactic centre Arches and Quintuplet clusters. *Monthly Notices of the Royal Astronomical Society*, 371:38–54, 2006. ISSN 0035-8711.

Q. D. Wang, H. Dong, A. Cotera, et al. HST/NICMOS Paschen-α Survey of the Galactic Centre: Overview. *Monthly Notices of the Royal Astronomical Society*, 402:895–902, 2010. ISSN 0035-8711.

Q. Yu and S. Tremaine. Ejection of Hypervelocity Stars by the (Binary) Black Hole in the Galactic Center. *The Astrophysical Journal*, 599:1129–1138, 2003. ISSN 0004-637X.

List of abbreviations

GC - Galactic Centre/galactocentric
H-R diagram - Hertzsprung-Russell diagram
IMF - initial mass function
NSC - Nuclear Star Cluster
PDMF - present-day mass function
SMBH - supermassive black hole
W-R stars - Wolf-Rayet stars
YNC - Young Nuclear Cluster